

**TWO HIGGS DOUBLET MODEL AND LEPTON POLARIZATION IN THE** **$B \rightarrow K\tau^+\tau^-$  DECAY**

T. M. ALİEV \*, M. SAVCI †, A. ÖZPİNECİ

Physics Department, Middle East Technical University

06531 Ankara, Turkey

H. KORU

Physics Department, Gazi University

06460 Ankara, Turkey

**Abstract**

The decay width, forward-backward asymmetry and  $\tau$  lepton longitudinal and transversal polarization for the exclusive  $B \rightarrow K\tau^+\tau^-$  decay in a two Higgs doublet model are computed. It is shown that the forward-backward asymmetry and longitudinal polarization of the  $\tau$  lepton are very effective tools for establishing new physics.

---

\*e-mail: taliev@rorqual.cc.metu.edu.tr

†e-mail: savci@rorqual.cc.metu.edu.tr

# 1 Introduction

The analysis of flavor changing neutral current (FCNC) decays is one of the most promising directions in particle physics, theoretical as well as experimental, as a potential testing ground for the Standard model (SM) and as regards to the physicists' endeavor to comply fully for establishing new physics beyond the SM [1]. Along these lines, the rare  $B$  meson decays which takes place via the FCNC, play an exceptional role. For example, an investigation of these rare decays opens the way for the possibility of a more precise determination of the Cabibbo-Kobayashi-Maskawa (CKM) matrix elements [2].

Currently the main interest on the rare meson decays is focused on the decays for which the SM predicts the largest branching ratios that can be measurable in the near future. The rare  $B \rightarrow K\ell^+\ell^-$  ( $\ell = e, \mu, \tau$ ) processes are such decays. For these decays the experimental situation is quite promising with  $e^+e^-$  and hadron colliders focusing only on the observation of exclusive modes with lepton pairs as the final states. The  $B \rightarrow K\ell^+\ell^-$ -decay, which is described by  $b \rightarrow s\ell^+\ell^-$  transition at quark level, has been investigated extensively in both SM and two Higgs doublet model (2HDM) [3]-[16]. It is well known that in the 2HDM, the up type quarks acquire their masses from Yukawa couplings to the Higgs doublet  $H_2$  (with the vacuum expectation value  $v_2$ ) and down type quarks and leptons acquire their masses from Yukawa couplings to the other Higgs doublet  $H_1$  (with the expectation value  $v_1$ ). In 2HDM there exist five physical Higgs fields: neutral scalar  $H^0, h^0$ , neutral pseudoscalar  $A^0$  and charged Higgs bosons  $H^\pm$ . Such a model occurs as natural a feature of the supersymmetric models [17]. In these models the interaction vertex of the Higgs boson and fermions depends on the ratio  $\tan\beta = \frac{v_2}{v_1}$  which is a free parameter in the model. The constraints on  $\tan\beta$  are usually obtained from  $B - \bar{B}$ ,  $K - \bar{K}$  mixing,  $b \rightarrow s\gamma$  decay width, semileptonic decay  $b \rightarrow c\tau\bar{\nu}_\tau$  and is given by [18, 19]:

$$0.7 \leq \tan\beta \leq 0.6 \left( \frac{m_{H^+}}{1 \text{ GeV}} \right), \quad (1)$$

(the lower bound  $m_{H^+} \geq 200 \text{ GeV}$  is obtained in [19]).

In all these studies the contributions from neutral Higgs boson exchange diagrams are neglected, since the lepton-lepton-Higgs vertices are proportional to the lepton mass. But for the  $b \rightarrow s\tau^+\tau^-$  decay the mass of the  $\tau$  lepton is not too small compared to the  $b$  quark mass, and hence one expects that the neutral Higgs boson exchange diagrams may contribute considerably to such channels. It has been pointed by Hewett [20] that the longitudinal polarization  $P_L$  of the final lepton is an important observable that may be accessible in the  $B \rightarrow K\tau^+\tau^-$ -decay mode. Recently it has been shown in [21] that the complementary information is contained in  $P_L$ , together with the two other orthogonal components of polarization ( $P_T$  is the component of of the polarization lying in the decay plane and  $P_N$  is the one that is normal to the decay plane). Both  $P_T$  and  $P_N$  are crucial for the  $\tau^+ \tau^-$  channel since they are proportional to  $\frac{m_\ell}{m_b}$ . The  $b \rightarrow s\ell^+\ell^-$  transition contains three Wilson coefficients  $C_7, C_9^{eff}$  and  $C_{10}$  in the SM. The different components of the polarization, i.e.,  $P_L, P_T$  and  $P_N$ , involve different combinations of Wilson coefficients  $C_7, C_9^{eff}$  and  $C_{10}$  (see below) and hence contain independent information. For this reason the polarization effects are thought to play an important role in further investigations of the structure of the SM and for establishing new physics beyond it.

The query for the calculation of the branching ratios and other observables requires the computation of the matrix element of the effective Hamiltonian responsible for the  $B \rightarrow K\tau^+\tau^-$  decay between  $B$  and  $K$  states. This problem is related to the non-perturbative sector of QCD and it can be solved only by means of a non-perturbative approach.

These matrix elements have been investigated in the framework of different approaches such as chiral theory [22], three point QCD sum rules method [23], relativistic quark model by the light-front formalism [24], effective heavy quark theory [25] and light cone QCD sum rules [26]. The aim of the present work is to calculate these matrix elements in the light cone QCD sum rules in the framework of the 2HDM, taking into account the newly appearing operators,  $C_{Q_i}$ , and to study the forward-backward asymmetry and final lepton polarization for the exclusive  $B \rightarrow K\tau^+\tau^-$  decay. Taking into account the additional neutral Higgs boson exchange diagrams, the effective Hamiltonian is calculated in [27] as

$$\mathcal{H}_{eff} = \frac{4G_F}{\sqrt{2}} V_{tb} V_{ts}^* \left\{ \sum_{i=1}^{10} C_i(\mu) O_i(\mu) + \sum_{i=1}^{10} C_{Q_i}(\mu) Q_i(\mu) \right\} , \quad (2)$$

where the first set of operators in the curly brackets describe the effective Hamiltonian responsible for the  $b \rightarrow sl^+l^-$  decay in the SM. Note that the contributions arising from the diagrams containing the charged Higgs bosons are taken into account by modifying the corresponding Wilson coefficients. These diagrams do not induce any additional operators. Their explicit forms and the corresponding Wilson coefficients  $C_i$  can be found in [6]. The second set of operators in the brackets, whose explicit forms are presented in [27], come from the exchange of the neutral Higgs bosons. The corresponding Wilson coefficients are:

$$\begin{aligned} C_{Q_1}(m_W) &= -\frac{m_b m_\ell}{m_{h^0}^2} \tan^2 \beta \frac{1}{\sin^2 \theta_W} \frac{x}{4} \left\{ (\sin^2 \alpha + h \cos^2 \alpha) f_1(x, y) + \right. \\ &+ \left[ \frac{m_{h^0}^2}{m_W^2} + (\sin^2 \alpha + h \cos^2 \alpha) (1 - z) \right] f_2(x, y) + \\ &+ \left. \frac{\sin^2 2\alpha}{2m_{H^\pm}^2} \left[ m_{h^0}^2 - \frac{(m_{h^0}^2 + m_{H^0}^2)^2}{2m_{H^0}^2} \right] f_3(y) \right\} , \end{aligned} \quad (3)$$

$$C_{Q_2}(m_W) = \frac{m_b m_\ell}{m_{A^0}^2} \tan^2 \beta \left\{ f_1(x, y) + \left[ 1 + \frac{m_{H^\pm}^2 - m_{A^0}^2}{m_W^2} \right] f_2(x, y) \right\} , \quad (4)$$

$$C_{Q_3}(m_W) = \frac{m_b e^2}{m_\ell g^2} \left[ C_{Q_1}(m_W) + C_{Q_2}(m_W) \right] , \quad (5)$$

$$C_{Q_4}(m_W) = \frac{m_b e^2}{m_\ell g^2} \left[ C_{Q_1}(m_W) - C_{Q_2}(m_W) \right] , \quad (6)$$

$$C_{Q_i}(m_W) = 0 \quad i = 5, \dots, 10 , \quad (7)$$

where

$$\begin{aligned}
x &= \frac{m_t^2}{m_W^2}, & y &= \frac{m_t^2}{m_{H^\pm}^2}, & z &= \frac{x}{y}, & h &= \frac{m_{h^0}^2}{m_{H^0}^2}, \\
f_1(x, y) &= \frac{x \ln x}{x-1} - \frac{y \ln y}{y-1}, & f_2(x, y) &= \frac{x \ln y}{(z-x)(x-1)} + \frac{\ln z}{(z-1)(x-1)}, \\
f_3(y) &= \frac{1-y+y \ln y}{(y-1)^2}.
\end{aligned}$$

The QCD correction to the Wilson coefficients  $C_i(m_W)$  and  $C_{Q_i}(m_W)$  can be calculated using the renormalization group equations. In [27] it was shown that the operators  $O_9$  and  $O_{10}$  do not mix with  $Q_i$  ( $i = 1, \dots, 10$ ), so that the Wilson coefficients  $C_9$  and  $C_{10}$  remain unchanged and their values are the same as in the SM. Their explicit forms can be found in [27], where it is also shown that  $O_7$  can mix with  $Q_i$ . But additional terms due to this mixing can safely be neglected since the corrections to the SM value of  $C_7$  arising from these terms are less than 5% when  $\tan\beta \leq 50$ .

Moreover the operators  $O_i$  ( $i = 1, \dots, 10$ ) and  $Q_i$  ( $i = 3, \dots, 10$ ) do not mix with  $Q_1$  and  $Q_2$  and also there is no mixing between  $Q_1$  and  $Q_2$ . For this reason the evolutions of the coefficients  $C_{Q_1}$  and  $C_{Q_2}$  are controlled by the anomalous dimensions of  $Q_1$  and  $Q_2$  respectively:

$$C_{Q_i}(m_b) = \eta^{-\gamma_Q/\beta_0} C_{Q_i}(m_W), \quad i = 1, 2,$$

where  $\gamma_Q = -4$  is the anomalous dimension of the operator  $\bar{s}_L b_R$ .

Neglecting the strange quark mass, the matrix element for  $b \rightarrow s\tau^+\tau^-$  decay is [27]:

$$\begin{aligned}
\mathcal{M} &= \frac{G_F \alpha}{2\sqrt{2}\pi} V_{tb} V_{ts}^* \left\{ C_9^{eff} \bar{s} \gamma_\mu (1 - \gamma_5) b \bar{\tau} \gamma^\mu \tau + C_{10} \bar{s} \gamma_\mu (1 - \gamma_5) b \bar{\tau} \gamma^\mu \gamma_5 \tau - \right. \\
&\quad \left. - 2C_7 \frac{m_b}{p^2} \bar{s} i \sigma_{\mu\nu} p^\nu (1 + \gamma_5) b \bar{\tau} \gamma^\mu \tau + C_{Q_1} \bar{s} (1 + \gamma_5) b \bar{\tau} \tau + C_{Q_2} \bar{s} (1 + \gamma_5) b \bar{\tau} \gamma_5 \tau \right\}, \quad (8)
\end{aligned}$$

where  $p^2$  is the invariant dileptonic mass, the Wilson coefficients  $C_7$ ,  $C_9$  and  $C_{10}$  are obtained from their SM values by adding the contributions due to the charged Higgs bosons exchange diagrams. Note that this addition is performed at high  $m_W$  scale, and then using the renormalization group equations, the coefficients are calculated at lower  $m_b$  scale. Coefficients  $C_{Q_1}$  and  $C_{Q_2}$  describe the neutral Higgs boson exchange diagrams' contributions. Note that the coefficient  $C_9^{eff}(\mu, p^2) \equiv C_9(\mu) + Y(\mu, p^2)$ , where the function  $Y$  contains the contributions from the one loop matrix element of the [6, 28, 29]. In addition to the short distance contributions, it is possible to take into account the long distance effects associated with real  $c\bar{c}$  in the intermediate states, i.e., with the cascade process  $B \rightarrow KJ/\psi(\psi') \rightarrow K\ell^+\ell^-$ . These contributions are taken into account by introducing a Breit-Wigner form of the resonance propagator and this procedure leads to an additional contribution to  $C_9^{eff}$  of the form [10, 30]

$$- \frac{3\pi}{\alpha^2} \sum_{V=J/\psi, \psi', \dots} \frac{m_V \Gamma(V \rightarrow \ell^+\ell^-)}{(p^2 - m_V^2) - im_V \Gamma_V}.$$

From eq.(8) it is obvious that, in order to calculate the decay width and other observables for the exclusive  $B \rightarrow K\ell^+\ell^-$  channel, the matrix elements  $\langle K | \bar{s} \gamma_\mu (1 - \gamma_5) b | B \rangle$ ,

$\langle K | \bar{s} i \sigma_{\mu\nu} q^\nu (1 + \gamma_5) b | B \rangle$ , and  $\langle K | \bar{s} (1 + \gamma_5) b | B \rangle$  have to be calculated. These matrix elements can be parametrized in terms of the formfactors  $f^+$ ,  $f^-$  and  $f_T$  in the following way:

$$\langle K(p_K) | \bar{s} \gamma_\mu (1 - \gamma_5) b | B(p_B) \rangle = (p_B + p_K)_\mu f^+(p^2) + p_\mu f^-(p^2), \quad (9)$$

$$\begin{aligned} \langle K(p_K) | \bar{s} i \sigma_{\mu\nu} p^\nu (1 + \gamma_5) b | B(p_B) \rangle &= \left[ (p_B + p_K)_\mu p^2 - \right. \\ &\quad \left. - p_\mu (m_B^2 - m_K^2) \right] \frac{f_T(p^2)}{m_B + m_K}, \end{aligned} \quad (10)$$

where  $p = p_B - p_K$  is the momentum transfer. To be able to calculate the the matrix element  $\langle K | \bar{s} (1 + \gamma_5) b | B \rangle$ , we multiply both sides of eq.(10) by  $p_\mu$  and use the equation of motion. Neglecting the mass of the strange quark, we get:

$$\langle K(p_K) | \bar{s} (1 + \gamma_5) b | B(p_B) \rangle = \left[ (m_B^2 - m_K^2) f^+(p^2) + p^2 f^-(p^2) \right] \frac{1}{m_b}. \quad (11)$$

Making use of eqs.(9), (10) and (11) we obtain for the matrix element of the  $B \rightarrow K \tau^+ \tau^-$  decay:

$$\mathcal{M} = \frac{G\alpha}{2\sqrt{2}\pi} V_{tb} V_{ts}^* \left\{ [A p_{K\mu} + B p_\mu] \bar{\ell} \gamma^\mu \ell + [C p_{K\mu} + D p_\mu] \bar{\ell} \gamma^\mu \gamma_5 \ell + F_1 \bar{\ell} \ell + F_2 \bar{\ell} \gamma_5 \ell \right\} \quad (12)$$

where

$$\begin{aligned} A &= 2 C_9^{eff} f^+ - C_7 \frac{4m_b f_T(p^2)}{m_B + m_K}, \\ B &= C_9^{eff} [f^-(p^2) + f^+(p^2)] + C_7 \frac{2m_b f_T(p^2) (m_B^2 - m_K^2 - p^2)}{p^2 (m_B + m_K)}, \\ C &= 2 C_{10} f^+(p^2), \\ D &= C_{10} [f^-(p^2) + f^+(p^2)], \\ F_1 &= C_{Q1} \frac{1}{m_b} [(m_B^2 - m_K^2) f^+(p^2) + p^2 f^-(p^2)], \\ F_2 &= C_{Q2} \frac{1}{m_b} [(m_B^2 - m_K^2) f^+(p^2) + p^2 f^-(p^2)]. \end{aligned} \quad (13)$$

The formfactors  $f^+(p^2)$ ,  $f^-(p^2)$  and  $f_T(p^2)$  are investigated in the light cone QCD sum rules framework and to a good accuracy their  $p^2$  dependence are found to be representable in the following pole forms [26]:

$$\begin{aligned} f^+(p^2) &= \frac{0.29}{\left(1 - \frac{p^2}{23.7}\right)}, \\ f^-(p^2) &= -\frac{0.21}{\left(1 - \frac{p^2}{24.3}\right)}, \\ f_T(p^2) &= -\frac{0.31}{\left(1 - \frac{p^2}{23}\right)}, \end{aligned} \quad (14)$$

which we will use in the numerical calculations. Using eq.(12) and performing summation over final lepton polarization, we get for the double differential decay rate:

$$\begin{aligned}
\frac{d\Gamma}{dp^2 dz} &= \frac{G^2 \alpha^2}{2^{12} \pi^5} \frac{|V_{tb} V_{ts}^*|^2 v \sqrt{\lambda}}{m_B} \left\{ \frac{1}{2} \lambda m_B^4 |A|^2 + \frac{1}{2} |C|^2 m_B^2 (\lambda m_B^2 + 16 m_\ell^2 r) + 2 |F_2|^2 m_B^2 s + \right. \\
&+ 8 \text{Re}(D^* F_2) m_B^2 m_\ell s + 8 |D|^2 m_B^2 m_\ell^2 s + 4 \text{Re}(C^* F_2) m_B^2 m_\ell (1 - r - s) + \\
&+ 8 \text{Re}(C^* D) m_B^2 m_\ell^2 (1 - r - s) + 2 |F_1|^2 m_B^2 s v^2 + z \left[ 4 \text{Re}(A^* F_1) \sqrt{\lambda} m_B^2 m_\ell v \right] - \\
&\left. - \frac{z^2}{2} \lambda m_B^4 v^2 (|A|^2 + |C|^2) \right\}, \tag{15}
\end{aligned}$$

where  $z = \cos\theta$  and  $\theta$  is the angle between the three momenta of the negatively charged lepton and the  $B$ -meson in the CM frame of the final leptons, and  $v = \sqrt{1 - \frac{4m_\ell^2}{p^2}}$  is the lepton velocity. Here  $\lambda(1, r, s)$  is the usual triangle function and  $r = \frac{m_K^2}{m_B^2}$ ,  $s = \frac{p^2}{m_B^2}$ . As we have noted previously, the forward-backward asymmetry  $A_{FB}$  and the final lepton polarization involve different combinations of the Wilson coefficients  $C_7$ ,  $C_9^{eff}$ ,  $C_{10}$ ,  $C_{Q_1}$ , and  $C_{Q_2}$  and therefore each of them contains independent information. For this reason, here in what follows we study these quantities in more detail.

The forward-backward asymmetry  $A_{FB}$  is defined as:

$$A_{FB}(p^2) = \frac{\int_0^1 dz \frac{d\Gamma}{dp^2 dz} - \int_{-1}^0 dz \frac{d\Gamma}{dp^2 dz}}{\int_0^1 dz \frac{d\Gamma}{dp^2 dz} + \int_{-1}^0 dz \frac{d\Gamma}{dp^2 dz}}.$$

Note that in the SM, the forward-backward asymmetry is zero when the polarization of the final lepton is summed over. The reason is obvious: the hadronic current for the  $B \rightarrow K$  transition is a pure vector current. But forward backward asymmetry (or charge asymmetry) is non-zero only if there exists C-violating terms. In the 2HDM there is a C-violating term proportional to  $F_1$  (see eq.(12)), so that,  $A_{FB}$  is nonzero and is proportional to the lepton mass. For small values of  $\tan\beta$ , the contributions from the neutral Higgs boson exchange diagrams are very small, and hence one expects that the value of  $A_{FB}$  be small also. But for large  $\tan\beta$ , the contributions of the neutral Higgs boson exchange diagrams become significant and we expect  $A_{FB}$  to be large. The numerical analysis confirms these expectations (see numerical analysis section).

Let us now discuss the lepton polarization effects. We define three orthogonal unit vectors:

$$\begin{aligned}
\vec{e}_L &= \frac{\vec{p}_1}{|\vec{p}_1|}, \\
\vec{e}_N &= \frac{\vec{p}_K \times \vec{p}_1}{|\vec{p}_K \times \vec{p}_1|}, \\
\vec{e}_T &= \vec{e}_N \times \vec{e}_L,
\end{aligned}$$

where  $\vec{p}_1$  and  $\vec{p}_K$  are the three momenta of the  $\ell^-$  lepton and the  $K$  meson, respectively, in the center of mass of the  $\ell^+ \ell^-$  system. The differential decay rate for any given spin

direction  $\vec{n}$  of the  $\ell^-$  lepton, where  $\vec{n}$  is a unit vector in the  $\ell^-$  lepton rest frame, can be written as

$$\frac{d\Gamma(\vec{n})}{dp^2} = \frac{1}{2} \left( \frac{d\Gamma}{dp^2} \right)_0 \left[ 1 + (P_L \vec{e}_L + P_N \vec{e}_N + P_T \vec{e}_T) \cdot \vec{n} \right], \quad (16)$$

where the subscript "0" corresponds to the unpolarized case, and  $P_L$ ,  $P_T$ , and  $P_N$ , which correspond to the longitudinal, transverse and normal components of the polarization vector, respectively, are functions of  $p^2$ . These components  $P_i$  ( $i = L, T, N$ ) are defined as:

$$P_i(p^2) = \frac{\frac{d\Gamma}{dp^2}(\vec{n} = \vec{e}_i) - \frac{d\Gamma}{dp^2}(\vec{n} = -\vec{e}_i)}{\frac{d\Gamma}{dp^2}(\vec{n} = \vec{e}_i) + \frac{d\Gamma}{dp^2}(\vec{n} = -\vec{e}_i)}. \quad (17)$$

The calculations for the  $P_i$ 's ( $i = L, T$ ) lead to the following results:

$$P_L = \frac{v}{\Delta} \left[ \frac{2}{3} \lambda m_B^4 \text{Re}(A^* C) - 4 \text{Re}(F_1^* F_2) m_B^2 s - 8 \text{Re}(D^* F_1) m_B^2 m_\ell s - 4 \text{Re}(C^* F_1) m_B^2 m_\ell (1 - r - s) \right], \quad (18)$$

$$P_T = \frac{\pi \sqrt{\lambda} m_B^3}{\sqrt{s} \Delta} \left[ m_\ell (1 - r - s) \text{Re}(A^* C) + s v^2 \text{Re}(C^* F_1) + s \text{Re}(A^* F_2) + 2 s m_\ell \text{Re}(A^* D) \right]. \quad (19)$$

The factor  $\Delta$  in eqs. (18) and (19) can be obtained from eq.(15) by an integration over  $z$  of the terms in the curly brackets. Note that the explicit form of the normal component  $P_N$  of the polarization vector of the  $\ell^-$  lepton is also calculated. However, an analysis of its behavior with respect to  $p^2$  shows that numerically it is quite small, so that we do not present it. As a check of our results, when we equate  $F_1$  and  $F_2$  to zero, i.e., neglect the contributions from the Higgs bosons, we obtain the results of [26].

## 2 Numerical Analysis

The values of the main input parameters, which appear in the expression for the decay width are:  $m_b = 5 \text{ GeV}$ ,  $m_c = 1.4 \text{ GeV}$ ,  $m_\tau = 1.78 \text{ GeV}$ ,  $m_\mu = 0.105 \text{ GeV}$ ,  $\Lambda_{QCD} = 225 \text{ MeV}$ ,  $m_B = 5.28 \text{ GeV}$ , and  $m_K = 0.495 \text{ GeV}$ . We use the pole form of the formfactors given in eq.(14). For  $B$  meson lifetime we take  $\tau(B_d) = 1.56 \times 10^{-12} \text{ s}$  [31]. The values of the Wilson coefficients  $C_7^{SM}(m_b)$  and  $C_{10}^{SM}(m_b)$  to the leading logarithmic approximation are [32, 33]:

$$C_7 = -0.315, \quad C_{10} = -4.642.$$

The expression  $C_9^{eff}$  for the  $b \rightarrow s$  transition in the next to leading order approximation is given as (see for example [32]):

$$\begin{aligned}
C_9^{eff}(m_b) = & C_9^{SM}(m_b) + C_9^{H^-}(m_b) + 0.124w(\hat{s}) + g(\hat{m}_c, \hat{s}) (3C_1 + C_2 + 3C_3 + C_4 + 3C_5 + C_6) - \\
& - \frac{1}{2}g(\hat{m}_q, \hat{s}) (C_3 + 3C_4) - \frac{1}{2}g(\hat{m}_b, \hat{s}) (4C_3 + 4C_4 + 3C_5 + C_6) + \\
& + \frac{2}{9} (3C_3 + C_4 + 3C_5 + C_6) , \tag{20}
\end{aligned}$$

with

$$C_1 = -0.249 , \quad C_2 = 1.108 , \quad C_3 = 1.112 \times 10^{-2} , \quad C_4 = -2.569 \times 10^{-2} ,$$

$$C_5 = 7.4 \times 10^{-3} , \quad C_6 = -3.144 \times 10^{-2} , \quad C_9^{SM}(m_b) = 4.227 ,$$

where  $\hat{m}_q = \frac{m_q}{m_b}$ ,  $\hat{s} = \frac{p^2}{m_b^2}$ . The explicit forms of  $C_7^{H^-}(m_W)$ ,  $C_9^{H^-}(m_W)$  and  $C_{10}^{H^-}(m_W)$  can be found in [5].

In the above expression  $w(\hat{s})$  represents the one gluon correction to the matrix element  $O_9$  and its explicit form can be found in [12], while the function  $g(\hat{m}_q, \hat{s})$  arises from the one loop contributions of the four quark operators  $O_1 - O_6$  (see for example [32, 33]), i.e.,

$$\begin{aligned}
g(\hat{m}_q, \hat{s}') = & -\frac{8}{9} \ln \hat{m}_q + \frac{8}{27} + \frac{4}{9} y_q - \frac{2}{9} (2 + y_q) \sqrt{11 - y_q} + \\
& + \left\{ \theta(1 - y_q) \left( \ln \frac{1 + \sqrt{1 - y_q}}{1 - \sqrt{1 - y_q}} - i\pi \right) + \theta(y_q - 1) \arctan \frac{1}{\sqrt{y_q - 1}} \right\} , \tag{21}
\end{aligned}$$

where  $y_q = \frac{\hat{m}_q}{\hat{s}'}$ , and  $\hat{s}' = \frac{4p^2}{m_b^2}$ .

In Table 1 we list the three different sets of values for the masses of the Higgs particles  $m_{h^0}$ ,  $m_{H^\pm}$ ,  $m_{H^0}$  and  $m_{A^0}$  that we use throughout the numerical calculations.

	$m_{h^0}$	$m_{H^\pm}$	$m_{H^0}$	$m_{A^0}$
mass set-1	80 GeV	200 GeV	150 GeV	100 GeV
mass set-2	250 GeV	300 GeV	100 GeV	350 GeV
mass set-3	100 GeV	400 GeV	200 GeV	150 GeV

Table 1: List of the values for the masses of the Higgs particles.



Further, we choose  $\sin\alpha = \frac{\sqrt{2}}{2}$  and the numerical calculations for the branching ratio are all carried at three different values of  $\tan\beta$ , i.e.,  $\tan\beta = 1$ ,  $\tan\beta = 20$  and  $\tan\beta = 30$ .

In Fig.1 (a) we present the  $p^2$  dependence of the differential branching ratio for the  $B_d \rightarrow K\tau^+\tau^-$  decay with the long distance effects, for  $\tan\beta = 1$ . The numbers 1, 2 and 3 on each curve identify the mass set-1, 2 and 3 for the Higgs particles  $m_{H^\pm}$ ,  $m_{h^0}$ ,  $m_{H^0}$  and  $m_{A^0}$ , respectively, as displayed in Table 1. The curve numbered as 4 is the one calculated in the Standard Model [26] and is depicted for a comparison of the two models. Fig.1 (b) and (c) are the similar graphs at  $\tan\beta = 20$  and  $\tan\beta = 30$ , respectively. The sharp peaks in these figures are due to the long distance contributions. Note that the curves that represent the short distance contributions are not plotted in this set of figures. The reason for this is our observation of the fact that, in each respective mass set these curves overlap with and mimic the behavior of the curves representing the long distance effects at all points of  $p^2$ , except at sharp peaks. It is also observed that the spectrum of the invariant mass distribution is slightly asymmetric.

In Fig.2 (a) and (b) we plot the dependence of the forward-backward asymmetry  $A_{FB}$  on  $p^2$  for the  $B_d \rightarrow K\tau^+\tau^-$  decay, with and without the long-distance effects at different values of  $\tan\beta$ . The lines numbered as 1, 3 and 5 represent the long distance effects for the mass sets 1, 2 and 3, respectively, while the lines with numbers 2, 4 and 6 are depicted for the short distance effects. From these figures we see that  $A_{FB}$  is negative for all values of  $p^2$  except in the  $\psi'$  resonance region and it is sensitive to the value of  $\tan\beta$ . For  $\tan\beta = 1$   $A_{FB}$  is quite small, so that we do not present it here.

In Fig.3 (a), (b) and (c) we present the  $p^2$  dependence of the longitudinal polarization of the final lepton  $P_L$  without the long distance effects at  $\tan\beta = 1$ ,  $\tan\beta = 30$  and  $\tan\beta = 50$ , respectively. The lines numbered as 1, 2 and 3 represent the mass set-1, 2 and 3, respectively. The line with number 4 is the one presented in [26] for the Standard Model calculations. As is obvious from these figures if we exclude the resonance mass region of  $\psi'$ ,  $P_L$  is negative for all values of  $p^2$ . Note that the behavior of the  $P_L$  curves are sensitive to the different choices of the value of  $\tan\beta$ .

In Fig.4 (a), (b) and (c) we present the  $p^2$  dependence of the transversal polarization  $P_T$  of the  $\tau$  lepton which lies in the decay plane, without the long distance effects, at  $\tan\beta = 1$ ,  $\tan\beta = 30$  and at  $\tan\beta = 50$ , respectively. The lines numbered as 1, 2 and 3 represent the mass set-1, 2 and 3, in the respective order. From these figures it follows that at  $\tan\beta = 1$   $P_T$  is positive at all values of  $p^2$ . On the other hand, for  $\tan\beta = 30$  and  $\tan\beta = 50$ ,  $P_T$  is positive near the threshold region while it becomes negative far from the threshold region. Therefore the determination of the sign of  $P_T$  in the future experiments is a very important issue and can provide a direct information for the establishment of new physics.

For completeness in Figs.5-7 we present the results for the  $B \rightarrow K\mu^+\mu^-$  decay. It is clear that in this case the neutral Higgs exchange diagram contributions are quite small and the deviation from the SM prediction is due to the charged Higgs boson exchange diagrams.

In Fig.5 we present the differential branching ratio versus  $p^2$  for  $B \rightarrow K\mu^+\mu^-$  with and without the long distance effects. The sharp peaks in these figures are due to the long distance contributions, as is the case for Fig.1. Fig.5 (a) is for the mass set-1, (b) is for the mass set-2 and (c) is presented for the mass set-3. The lines numbered as 1, 3 and 5 represent the long distance effects for the mass sets 1, 2 and 3, respectively, while the numbers 2, 4 and 6 are presented for the short distance effects. The abbreviation *SM* on

the bottom pair of curves (5 and 6) stands for the Standard Model results as depicted in [26]. The branching ratio for the  $B \rightarrow K\mu^+\mu^-$  decay is not as sensitive to the value of  $\tan\beta$  as for the  $B \rightarrow K\tau^+\tau^-$  decay.

The behavior of the longitudinal polarization  $P_L$  with changing  $p^2$  for the  $B \rightarrow K\mu^+\mu^-$  decay is presented in Fig.6, with and without the long distance effects. Curves 1, 2 are evaluated numerically at  $\tan\beta = 1$  while those 3 and 4 represents the behavior of the longitudinal polarization calculated at  $\tan\beta = 50$ . The last two curves 5 and 6 depict the Standard Model results [26]. The ordering of the figures and of the numbering of lines for the short and long distance effects are exactly the same as explained for Fig.5. Without the long distance effects  $P_L$  is always negative.

In Fig.7 (a), (b) and (c) we present the transversal polarization  $P_T$  for the  $B \rightarrow K\mu^+\mu^-$  decay as a function of  $p^2$ , for mass set-1, mass set-2 and mass set-3, respectively. While at  $\tan\beta = 1$   $P_T$  is always positive, at  $\tan\beta = 30$  and  $\tan\beta = 50$  it changes sign. Thus the investigation of the sign of  $P_T$  can be an effective tool in search for new physics.

Since, as we have already noted,  $A_{FB}$ ,  $P_L$ , and  $P_T$  contain independent information, their investigation in the future experiments will be quite an efficient tool for establishing new physics.

In Table 2 we present the values of the branching ratios for the  $B_d \rightarrow K\tau^+\tau^-$  decay. After integrating over  $p^2$  we get for the branching ratios for the  $B_d \rightarrow K\tau^+\tau^-$  decay, with the long distance contributions:

	$\tan\beta = 1$	$\tan\beta = 20$	$\tan\beta = 30$
mass set-1	$3.47 \times 10^{-7}$	$2.68 \times 10^{-7}$	$4.12 \times 10^{-7}$
mass set-2	$3.15 \times 10^{-7}$	$2.64 \times 10^{-7}$	$3.71 \times 10^{-7}$
mass set-3	$2.96 \times 10^{-7}$	$3.01 \times 10^{-7}$	$5.43 \times 10^{-7}$

Table 2: Branching ratios for the exclusive  $B_d \rightarrow K\tau^+\tau^-$  decay, with the long distance contributions.

The ratio of the exclusive and inclusive channels is defined as:

$$R = \frac{B(B_d \rightarrow K\tau^+\tau^-)}{B(b \rightarrow s\tau^+\tau^-)}.$$

In the SM this ratio is given as  $R = 0.07 \pm 0.02$  when  $B(b \rightarrow s\tau^+\tau^-) = (2.6 \pm 0.5) \times 10^{-7}$  [33]. In Table 3 we display the results that we have calculated for our case, using the values given in Table 2.

	$\tan\beta = 1$	$\tan\beta = 20$	$\tan\beta = 30$
mass set-1	1.33	1.03	1.58
mass set-2	1.21	1.02	1.43
mass set-3	1.14	1.16	2.09

Table 3: The ratio  $R$  of the exclusive  $B(B_d \rightarrow K\tau^+\tau^-)$  and SM value of the inclusive  $B(b \rightarrow s\tau^+\tau^-)$  channels.

where we have used the SM value for the inclusive  $B(b \rightarrow s\tau^+\tau^-)$ .

For completeness we present in Table 4 the branching ratio with respect to the inclusive  $B(b \rightarrow s\tau^+\tau^-)$  decay in 2HDM with the long distance contributions. The expression for the inclusive  $B(b \rightarrow s\tau^+\tau^-)$  decay is given in [27].

	$\tan\beta = 1$	$\tan\beta = 20$	$\tan\beta = 30$
mass set-1	$18.90 \times 10^{-7}$	$17.97 \times 10^{-7}$	$18.44 \times 10^{-7}$
mass set-2	$18.61 \times 10^{-7}$	$17.98 \times 10^{-7}$	$18.34 \times 10^{-7}$
mass set-3	$18.44 \times 10^{-7}$	$18.13 \times 10^{-7}$	$18.98 \times 10^{-7}$

Table 4: Branching ratios for the inclusive  $B_d \rightarrow K\tau^+\tau^-$  decay in the 2HDM, with the long distance contributions.

Finally in Table 5, we display the results for the ratio  $R$  of the inclusive  $B(b \rightarrow s\tau^+\tau^-)$  decay calculated in the 2HDM and SM value of the inclusive  $B(b \rightarrow s\tau^+\tau^-)$  channel.

	$\tan\beta = 1$	$\tan\beta = 20$	$\tan\beta = 30$
mass set-1	7.27	6.91	7.09
mass set-2	7.16	6.92	7.05
mass set-3	7.09	6.97	7.30

Table 5: The ratio  $R$  of the inclusive  $B(b \rightarrow s\tau^+\tau^-)$  decay in 2HDM and SM.

In conclusion, we calculate the rare  $B \rightarrow K\ell^+\ell^-$  decay in 2HDM. It is observed that the forward-backward asymmetry  $A_{FB}$ , the longitudinal polarization  $P_L$  and the transversal polarization  $P_T$  of the charged final lepton are very sensitive to the variations in  $\tan\beta$ . Therefore, in search of new physics their experimental investigation can serve as the crucial test.

## Figure Captions

1. Invariant mass distribution for the  $B \rightarrow K\tau^+\tau^-$  decay with the long distance effects. In Fig.1 (a), (b) and (c) the numbers 1, 2 and 3 on each curve identify the mass set-1, 2 and 3, respectively, for the Higgs particles. The curve numbered as 4 is the one calculated in the Standard Model. The sharp peaks in these figures are all due to the long distance contributions.

2. The dependence of the forward-backward asymmetry  $A_{FB}$  on  $p^2$  for the decay  $B \rightarrow K\tau^+\tau^-$ . The lines numbered as 1,3 and 5 represent the long distance effects for the mass sets 1, 2 and 3, respectively, while the lines with numbers 2, 4 and 6 are chosen for the short distance effects.

3. The dependence of the longitudinal polarization,  $P_L$ , on  $p^2$  for the  $B \rightarrow K\tau^+\tau^-$  without the long distance effects. The lines numbered as 1, 2 and 3 represent the mass set-1, 2 and 3, respectively. The line with number 4 is the one presented for the Standard Model calculations.

4. Transversal polarization asymmetry,  $P_T$ , for the  $B \rightarrow K\tau^+\tau^-$  decay as a function of  $p^2$ . In this set of figures the lines numbered as 1, 2 and 3 represent the mass set-1, 2 and 3, respectively.

5. The same as in Fig.1, but for the  $B \rightarrow K\mu^+\mu^-$  decay. Fig.5 (a) is for mass set-1, (b) is for mass set-2 and (c) is presented for mass set-3. The lines numbered as 1, 3 and 5 represent the long distance effects for the mass sets 1, 2 and 3, respectively, while the numbers 2, 4 and 6 are presented for the short distance effects. The abbreviation *SM* on the bottom pair of curves (5 and 6) stands for the Standard Model results.

6. The same as in Fig.3 but for the  $B \rightarrow K\mu^+\mu^-$  decay. The ordering of the figures and of the numbering of lines are exactly the same as explained for Fig.5.

7. The same as in Fig.4, but for the  $B \rightarrow K\mu^+\mu^-$  decay. Figures (a), (b) and (c) are presented for the mass set-1, mass set-2 and mass set-3, respectively.

al

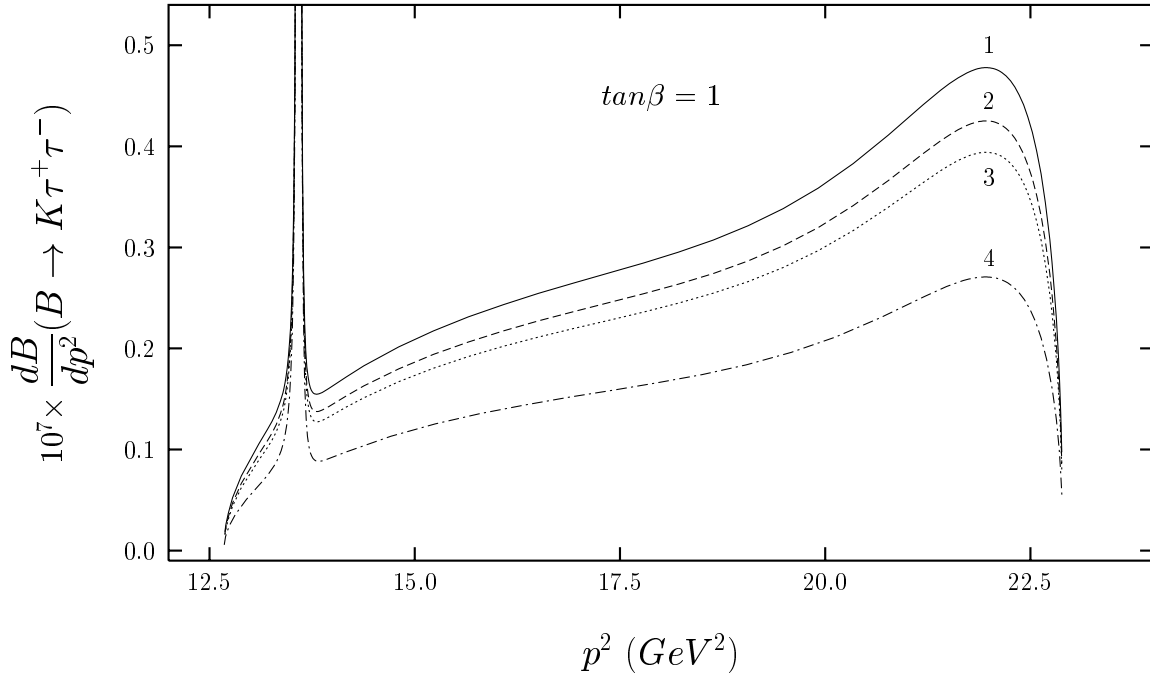


**Fig.1 (a)**

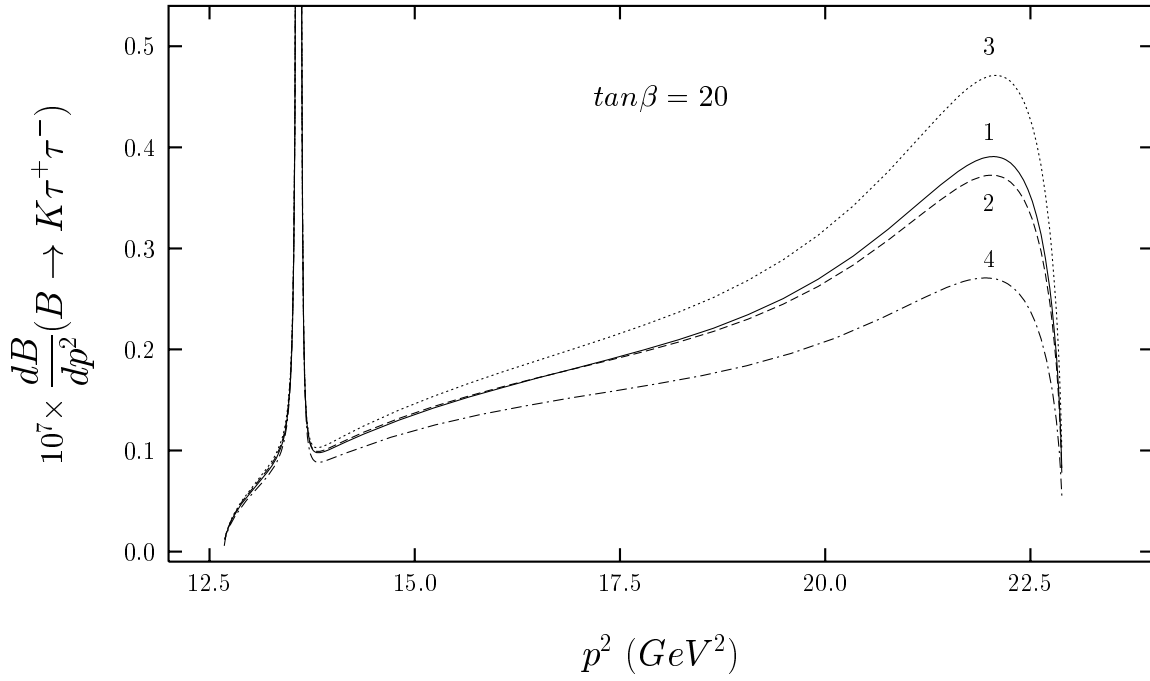


**Fig.1 (b)**

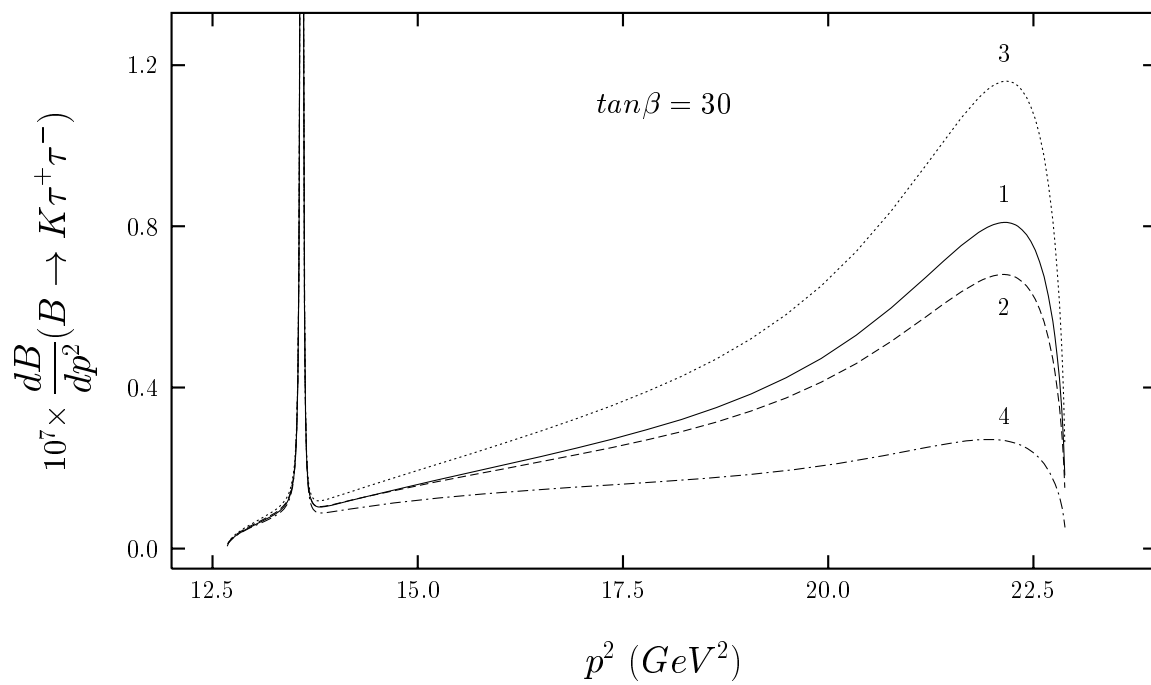


**Fig.1 (c)**

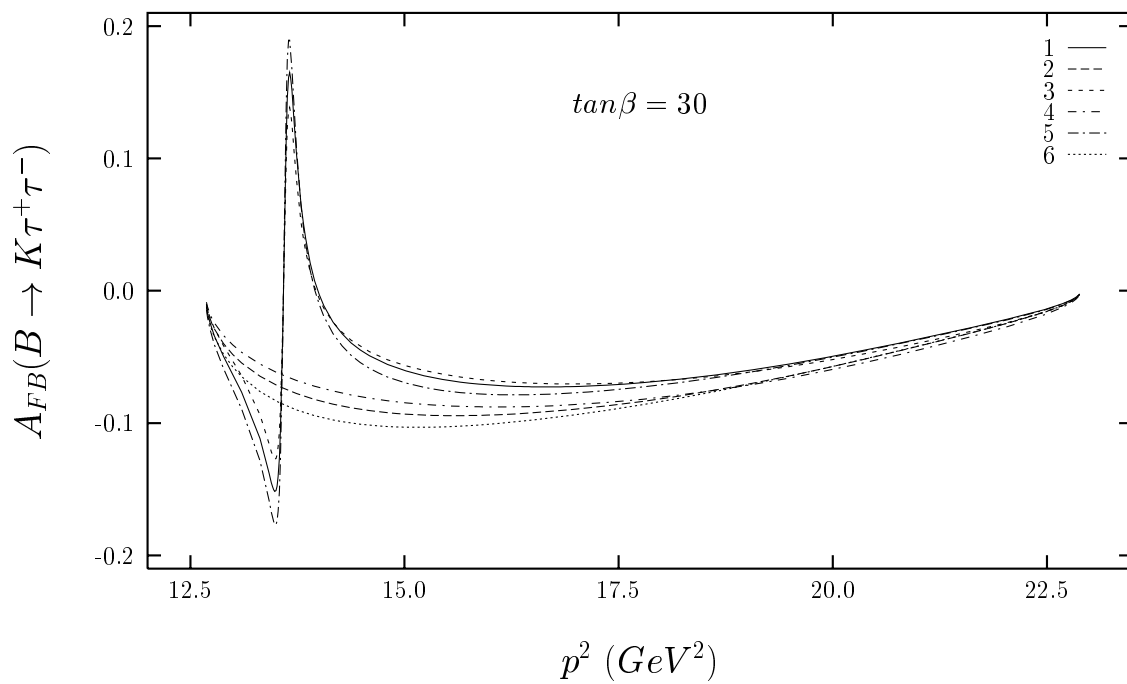


**Fig.2 (a)**

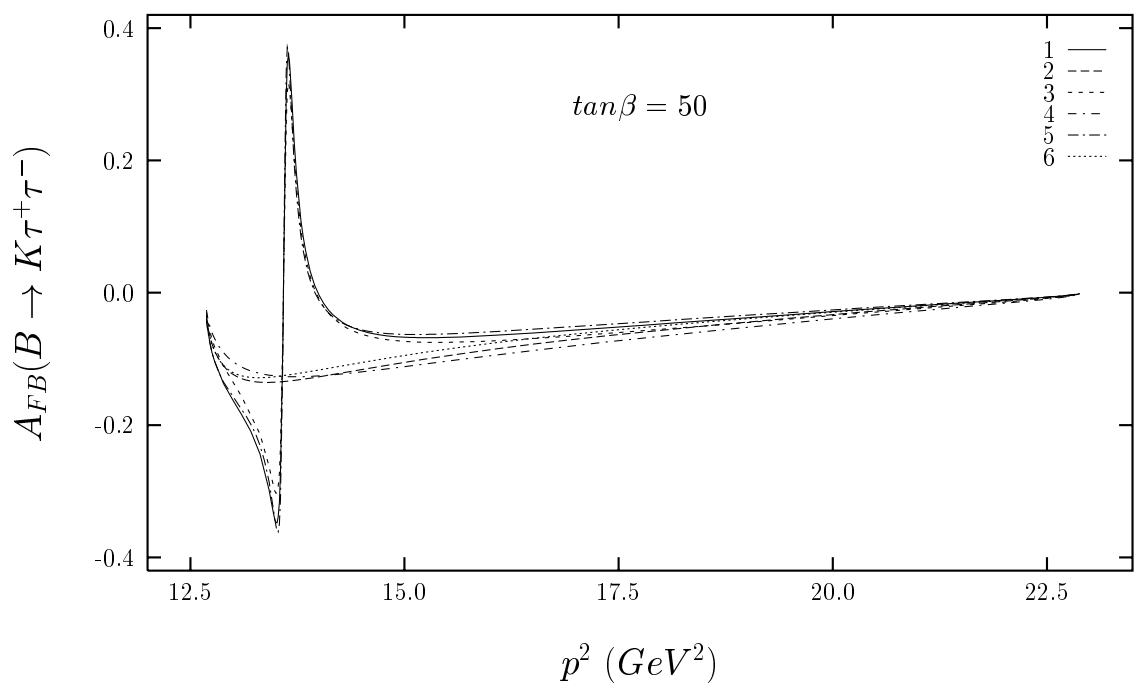


**Fig.2 (b)**

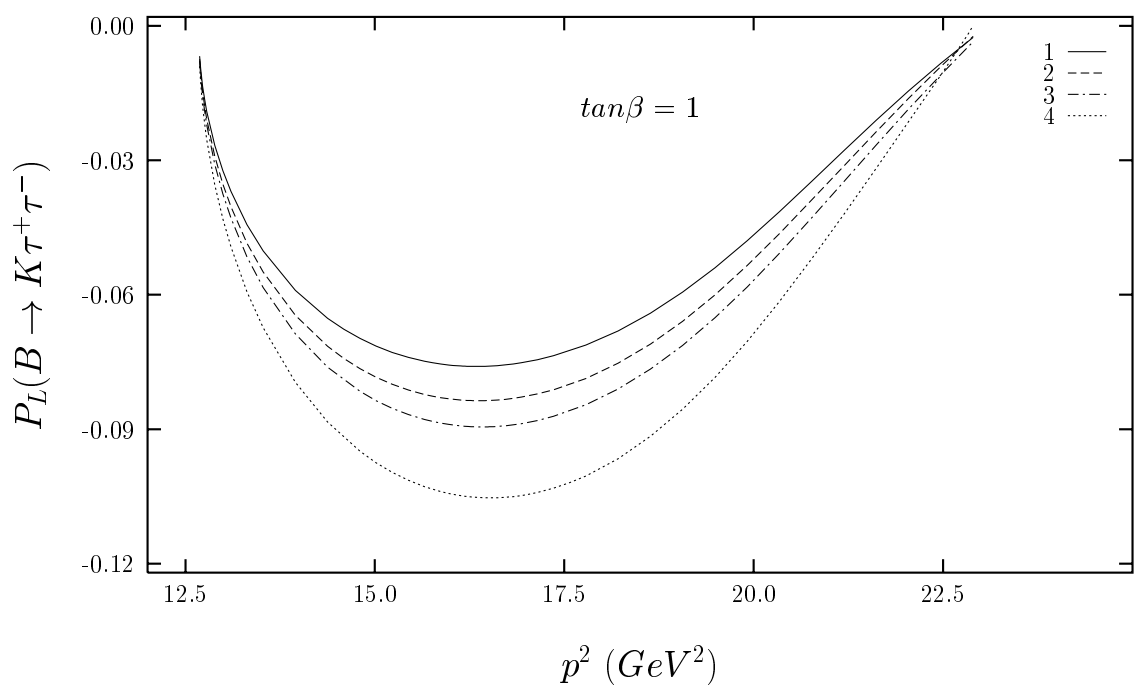


**Fig.3 (a)**



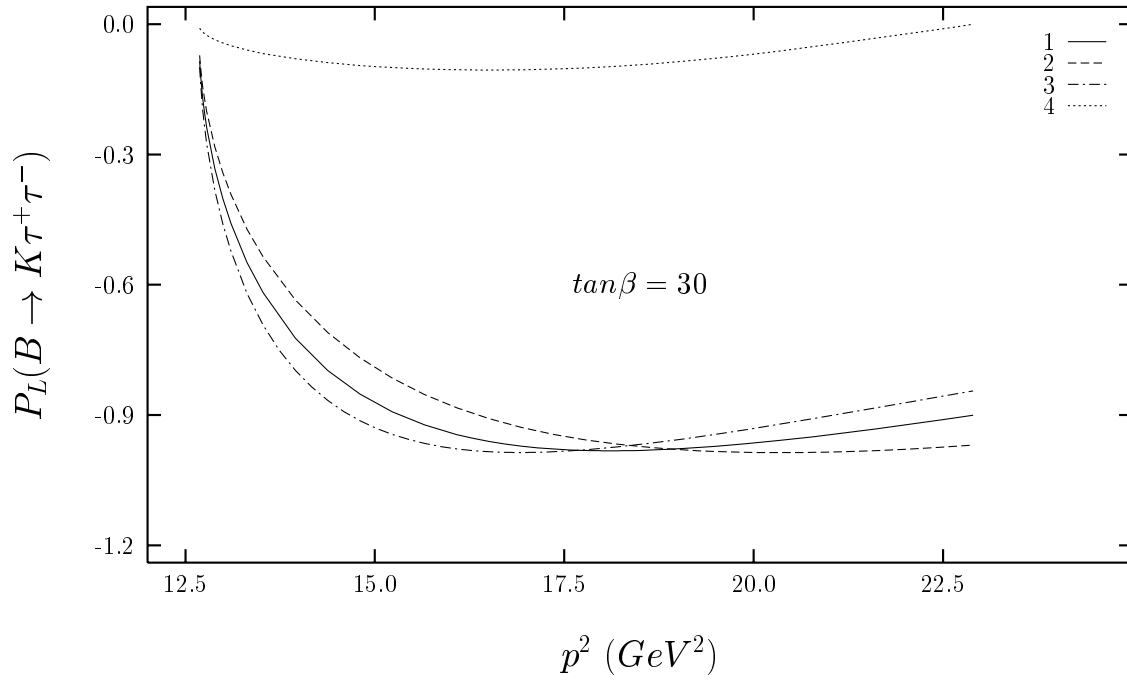


**Fig.3 (b)**

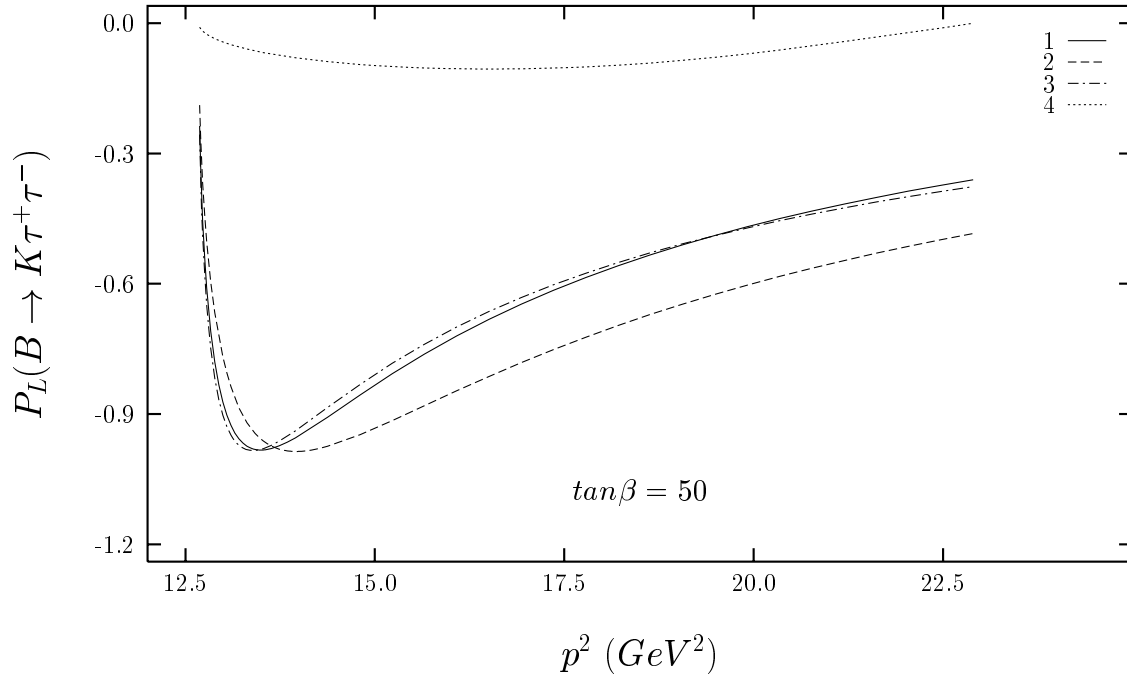


**Fig.3 (c)**

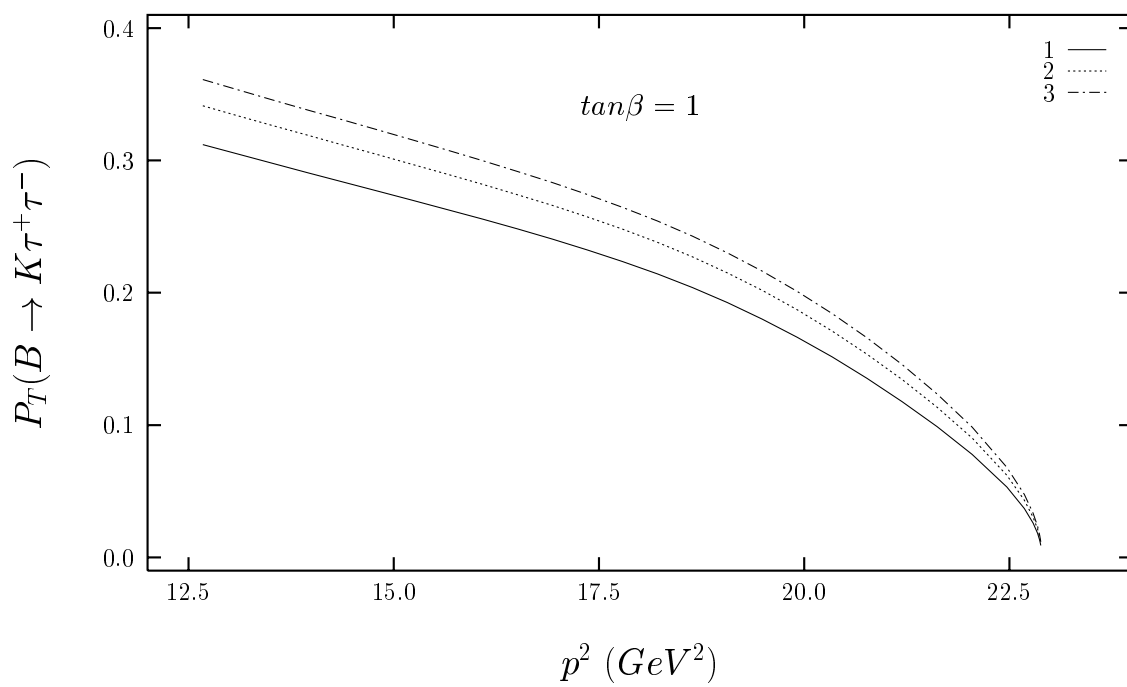


**Fig.4 (a)**

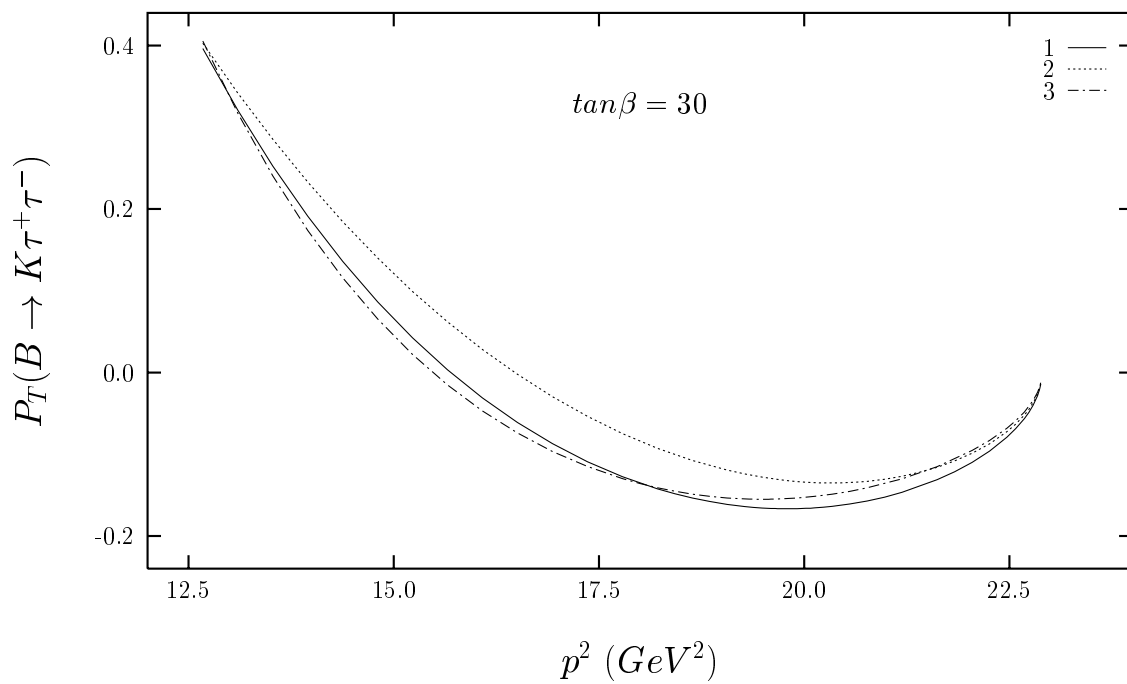


**Fig.4 (b)**

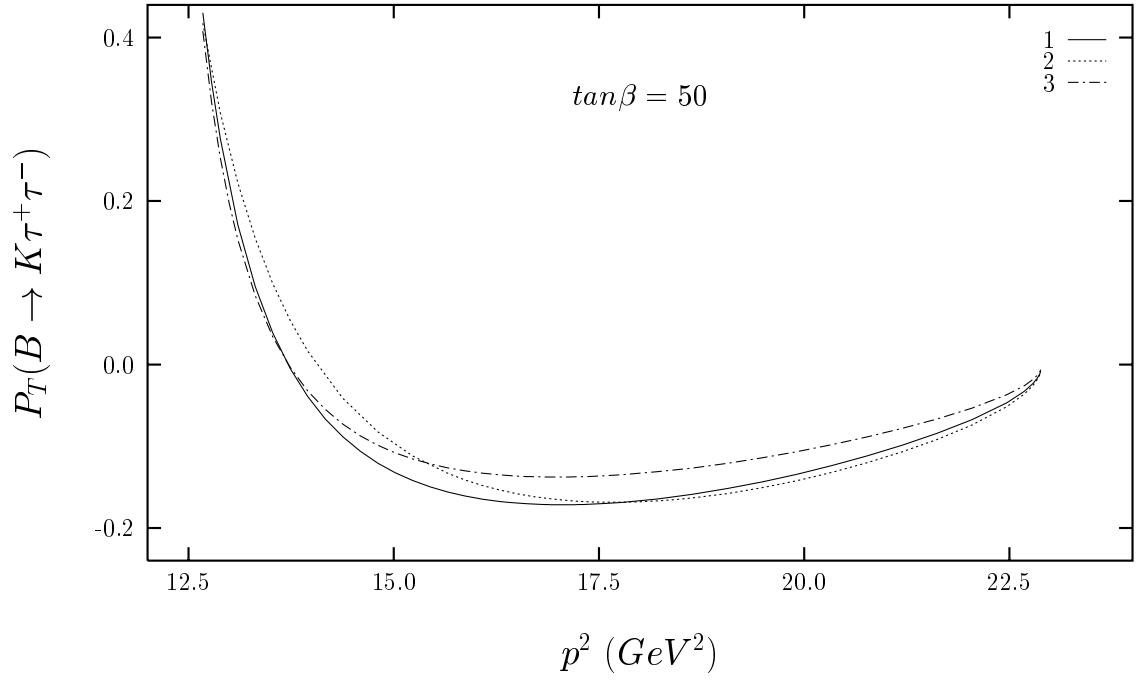


**Fig.4 (c)**

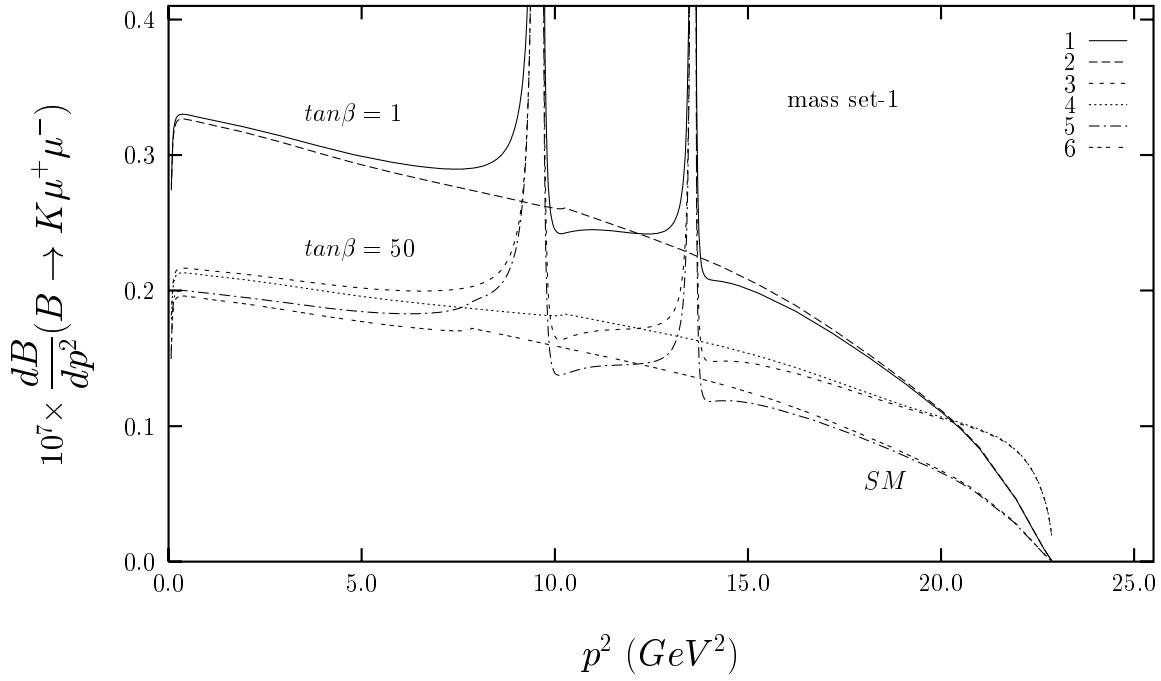


**Fig.5 (a)**

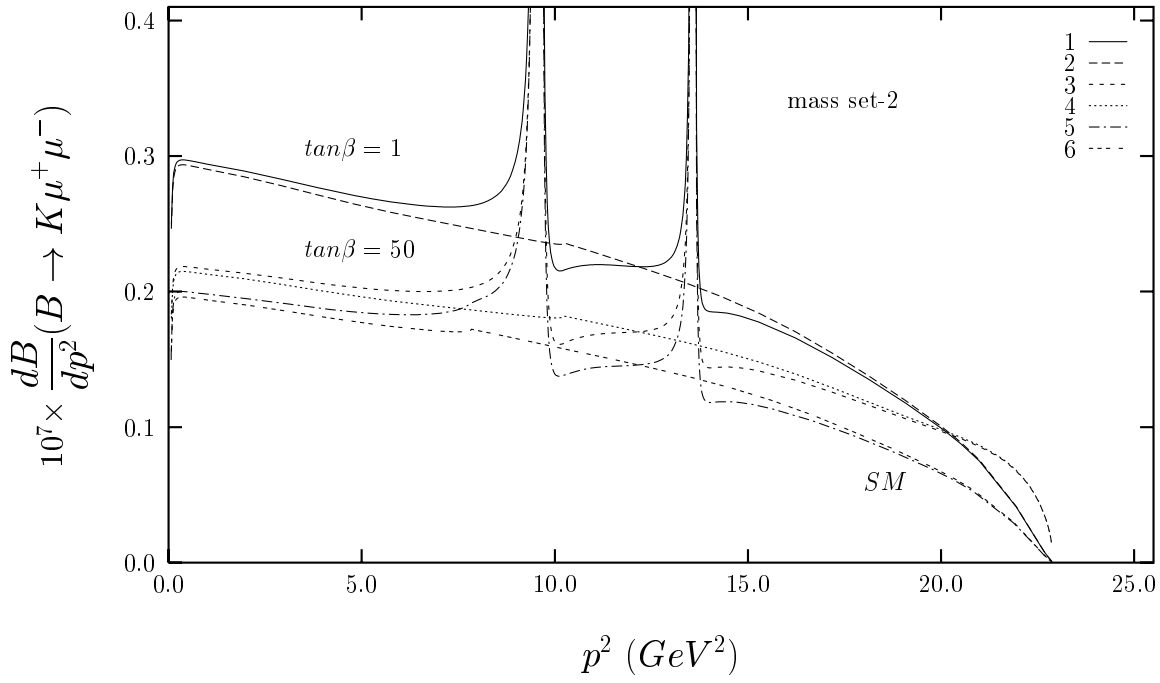


**Fig.5 (b)**

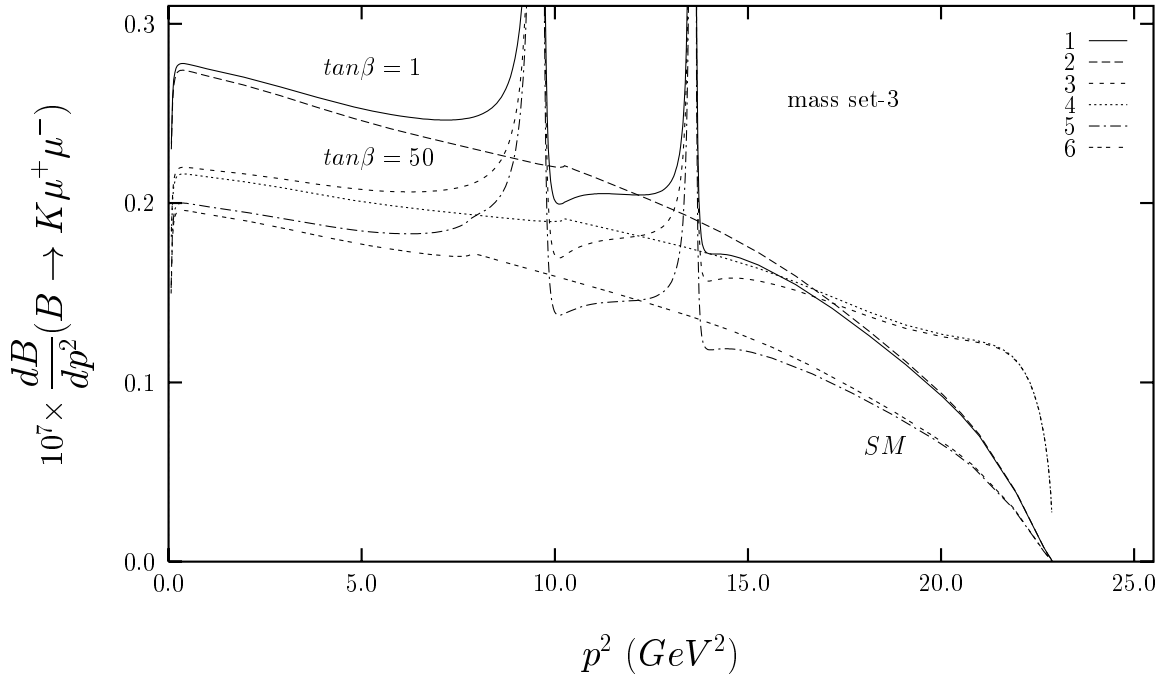


**Fig.5 (c)**

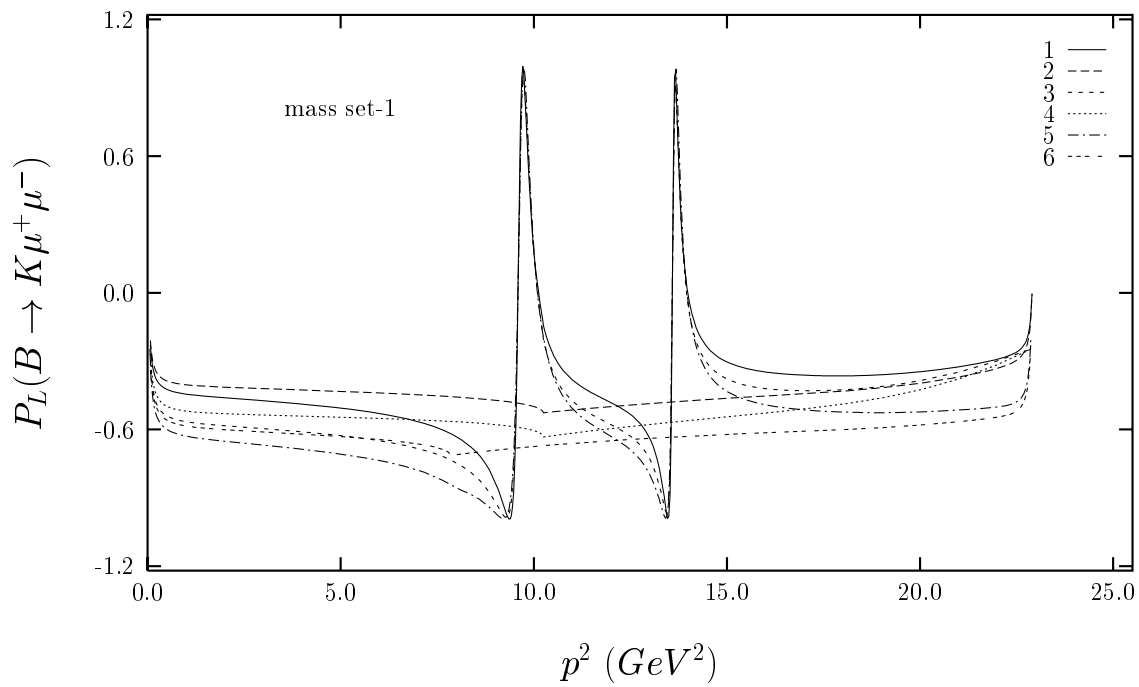


**Fig.6 (a)**

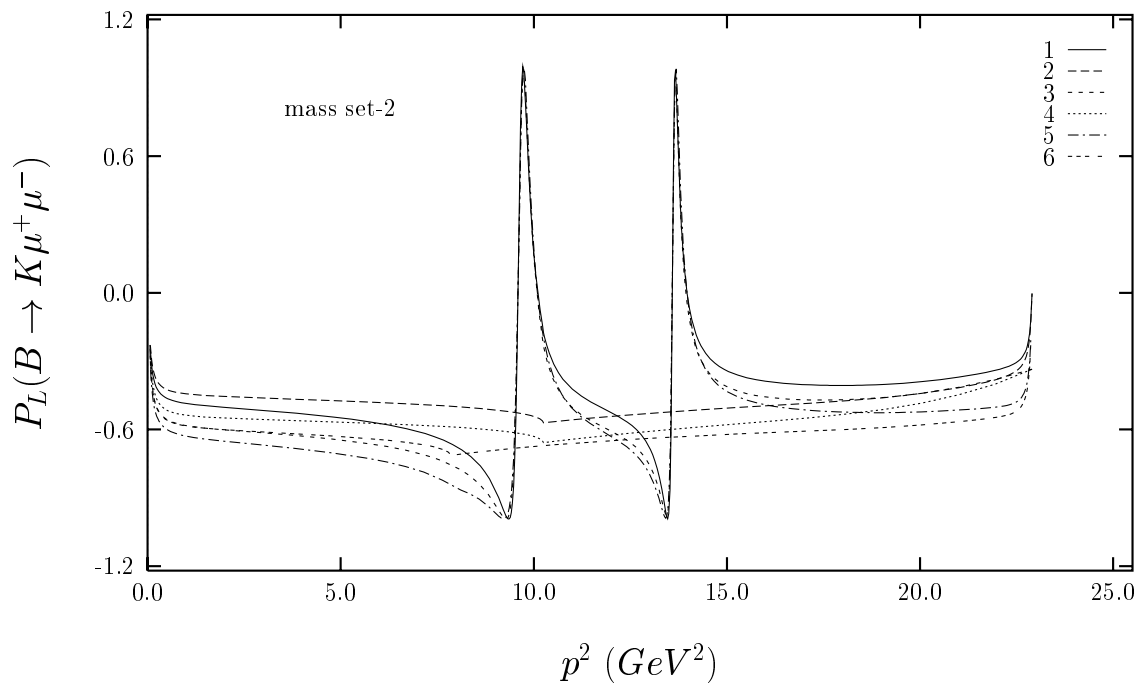


**Fig.6 (b)**

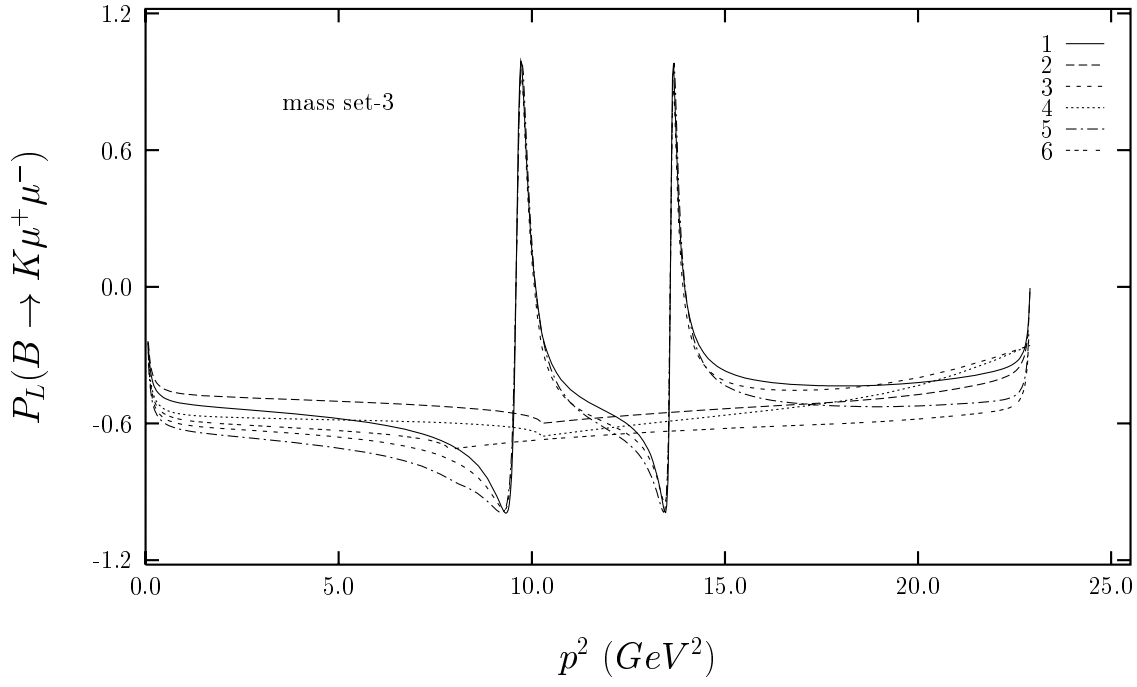


**Fig.6 (c)**

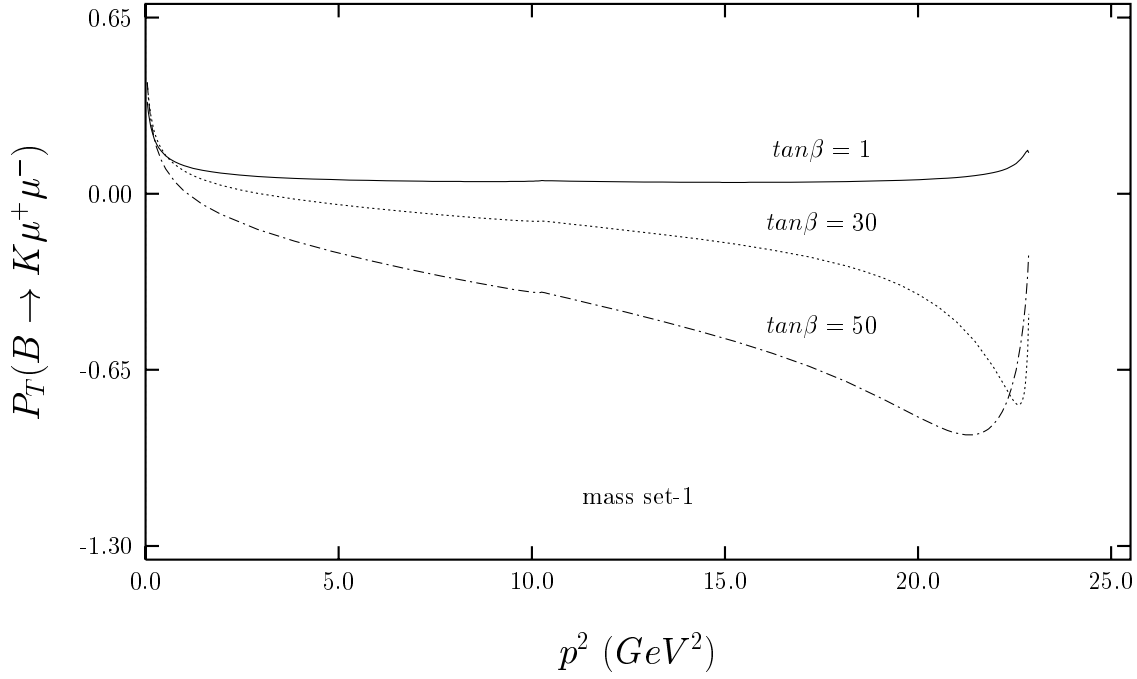


**Fig.7 (a)**

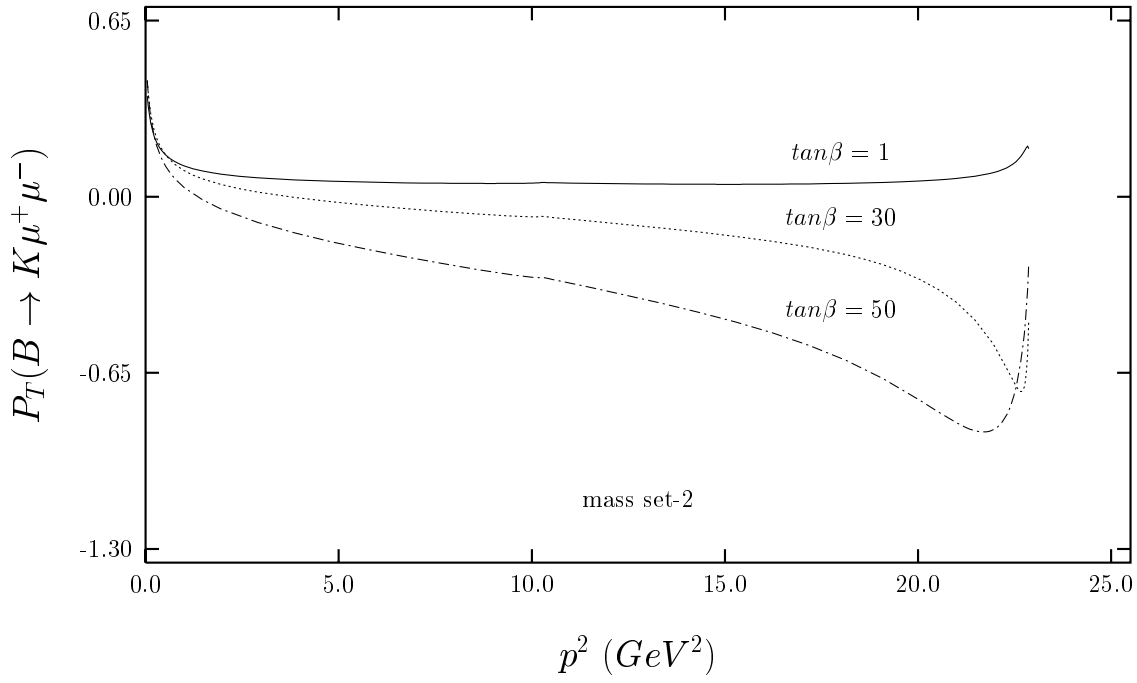


**Fig.7 (b)**

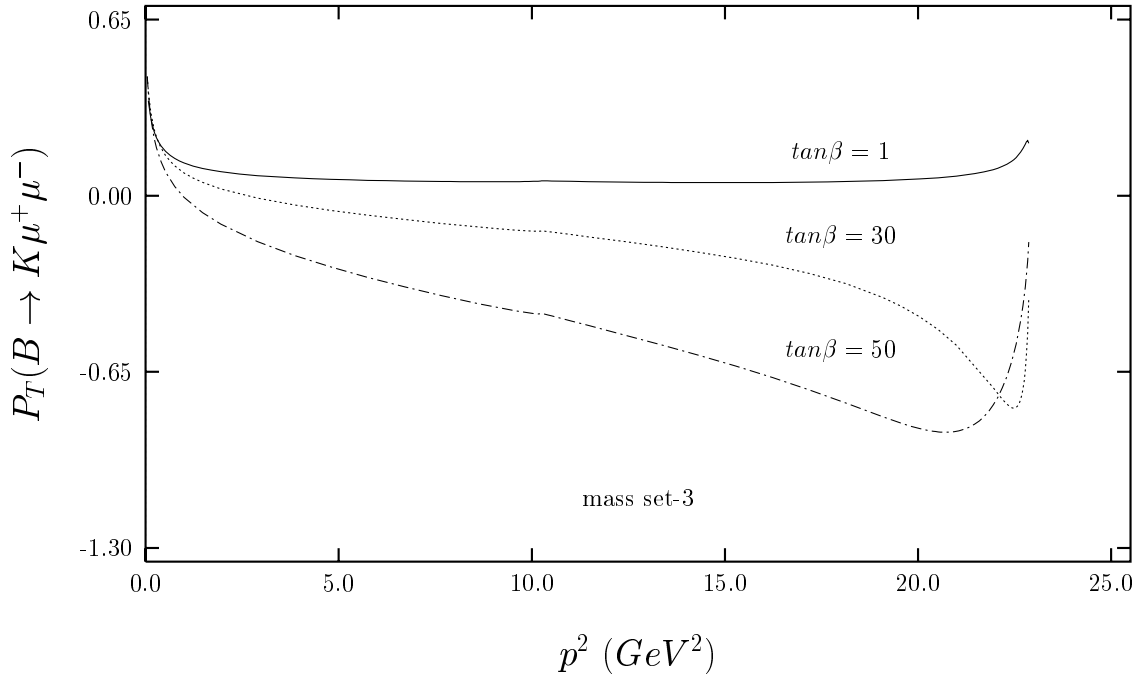


**Fig.7 (c)**

## References

- [1] C. Anway-Wiese, **CDF** Collaboration, in: *Proc. of the 8<sup>th</sup> Meeting of the Division of Particle and Fields of the American Physical Society*, Albuquerque, New Mexico, 1994, ed: S. Seidel (World Scientific, Singapore, 1995).
- [2] Z. Ligeti and M. Wise, *Phys. Rev.* **D53** (1996) 4937;
- [3] W. -S. Hou, R. S. Willey and A. Soni, *Phys. Rev. Lett.* **58** (1987) 1608.
- [4] N. G. Deshpande and J. Trampetic, *Phys. Rev. Lett.* **60** (1988) 2583.
- [5] C. S. Lim, T. Morozumi and A. I. Sanda, *Phys. Lett.* **B218** (1989) 343.
- [6] B. Grinstein, M. J. Savage and M. B. Wise, *Nucl. Phys.* **B319** (1989) 271.
- [7] C. Dominguez, N. Paver and Riazuddin, *Phys. Lett.* **B214** (1988) 459.
- [8] N. G. Deshpande, J. Trampetic and K. Ponose, *Phys. Rev.* **D39** (1989) 1461.
- [9] W. Jaus and D. Wyler, *Phys. Rev.* **D41** (1990) 3405.
- [10] P. J. O'Donnell and H. K. Tung, *Phys. Rev.* **D43** (1991) 2067.
- [11] N. Paver and Riazuddin, *Phys. Rev.* **D45** (1992) 978.
- [12] A. Ali, T. Mannel and T. Morozumi, *Phys. Lett.* **B273** (1991) 505.
- [13] A. Ali, G. F. Giudice and T. Mannel, *Z. Phys.* **C67** (1995) 417.
- [14] C. Greub, A. Ioannissian and D. Wyler, *Phys. Lett.* **B346** (1995) 145;  
D. Liu *Phys. Lett.* **B346** (1995) 355;  
G. Burdman, *Phys. Rev.* **D52** (1995) 6400;  
Y. Okada, Y. Shimizu and M. Tanaka **hep-ph/9704223**.
- [15] A. J. Buras and M. Münz, *Phys. Rev.* **D52** (1995) 186.
- [16] N. G. Deshpande, X. -G. He and J. Trampetic, *Phys. Lett.* **B367** (1996) 362.
- [17] J. F. Gunion, H. E. Haber, G.Kane and S. Dawson, "*The Higgs Hunters Guide*", (Addison-Wesley Reading, MA, 1990).
- [18] A. K. Grant, *Phys. Rev.* **D51** (1995) 207.
- [19] J. Kalinowski, *Phys. Lett.* **B245** (1990) 201.
- [20] J. L. Hewett, *Phys. Rev.* **D53** (1996) 4964.
- [21] F. Krüger and L. M. Sehgal, *Phys. Lett.* **B380** (1996) 199.
- [22] R. Casalbuoni, A. Deandrea, N. Di Bartolomeo, R. Gatto and G. Nardulli, *Phys. Lett.* **B312** (1993) 315.



- [23] P. Colangelo, F. De Fazio, P. Santorelli and E. Scrimieri, *Phys. Rev.* **D53** (1996) 3672.
- [24] W. Jaus and D. Wyler, *Phys. Rev.* **D41** (1990) 3405.
- [25] W. Roberts, *Phys. Rev.* **D54** (1996) 863.
- [26] T. M. Aliev, H. Koru, A. Özpineci and M. Savcı, *Phys. Lett.* **B400** (1997) 194.
- [27] Yuan-Ben Dai, Chao-Shang Huang and Han-Wen Huang,  
*Phys. Lett.* **B390** (1997) 257.
- [28] M. Misiak, *Nucl. Phys.* **B398** (1993) 23; Erratum: *ibid* **B439** (1995) 461.
- [29] A. J. Buras and M. Münz, *Phys. Rev.* **D52** (1995) 186;  
M. Ciuchini, E. Franco, G. Martinelli, L. Reina and L. Silvestrini,  
*Phys. Lett.* **B316** (1993) 127;  
M. Ciuchini, E. Franco, G. Martinelli and L. Reina, *Nucl. Phys.* **B415** (1994) 403;  
G. Cella, G. Curci, R. Ricciardi and A. Vicere, *Nucl. Phys.* **B421** (1994) 41;  
*ibid Phys. Lett.* **B325** (1994) 227.
- [30] A. I. Vainshtein, V. I. Zakharov, L. B. Okun and M. A. Shifman,  
*Sov. J. Nucl. Phys.* **24** (1976) 427.
- [31] Particle Data Group, *Phys. Rev.* **D54** (1996).
- [32] F. Krüger and L. M. Sehgal, *Phys. Rev.* **D55** (1997) 2799.
- [33] A. Ali, *Prep.* **DESY 97-019**; **hep-ph/9702312** (1997).